Effects of Rough Hail Scattering on Polarimetric Variables

Djordje Mirkovic, Dusan S. Zrnic, *Life Fellow, IEEE*, Valery Melnikov and Pengfei Zhang

Abstract— **We use a commercially available full-wave electromagnetic tool to model scattering off rough hail. Through modeling various axis ratios and surface roughness, we systematically evaluate their effect on the polarimetric variables used for hail size discrimination. Our results produce the differential reflectivity and the copolar correlation coefficient typically not achieved using forward operators. We compare our results with available information in the literature. Inclusion of the additional shape parameter brings new insight on problems associated with the polarimetric variable for hailstone size gauging. Finally, using WSR-88Ds' observations of a hail storm on two opposite sides, we hypothesize that the source of negative differential reflectivity is wet oblate hail in the resonant size range.**

***Index Terms*—Polarimetric weather radar, polarimetric variables, scattering from hail, hail observations, hail signature.**

I. Introduction

In the US and worldwide, hail is one of the most destructive and costly high-impact weather phenomena. According to [1], from 2000 through 2013, insurers paid more than $54 billion for hail incurred damage. Between 2014 and 2017, the damage was over $ 72 billion [2]. That means that more than $7 billion per year is the average from 2000 through 2017. This is over twice the average damage of $2.7 billion caused by tornadoes from 2000 through 2019. Although tornado warnings save lives, property in the path of a tornado cannot be saved. This, however, is not the case with hail warnings. These can reduce damage to the transportation industry (aircraft, boats) and the public; citizens can shelter cars in garages or avoid travel through a hailstorm. Large and giant hail causes the greatest damage. Hence it is important to predict its occurrence.

Hail detection and estimation of size is a crucial part of the National Weather Service (NWC) mission. NWS designates hail larger than 25 mm (1 in) as "severe" and hail larger than 50 mm as "significantly severe" [3]. For short-term nowcasting and warning, the NWS uses its network of dual-polarization weather radars (WSR-88D) as well as reports by the public and storm spotters. To educate the public and obtain quantitative information about size, the NWS has a list of size categories of hail. Each category is paired with a familiar object like a penny with 3/4 in, a quarter with 1 in, an egg with 2 in, a tennis ball with 2.5 in, etc., and the total number of categories between 0.5 in and larger than 4.5 in is fourteen (see NOAA hail size comparison chart [4]). Although dual-polarization has enabled significant improvement in detecting hail [5], gauging its size remains challenging.

Dual polarization weather radar has been used for the detection of hail for over 30 years. Reference [6] presents a comprehensive discussion of hail's polarimetric properties suitable for discriminating it from other hydrometeors. The increase in circular depolarization ratio C_{DR} and equivalent reflectivity factor caused by hail is a proven polarimetric indicator of hail [7]. Later studies relied on the reflectivity factor and the differential reflectivity [8], [9], [10], and the second polarimetric method for hail identification is based on this pair. Hail causes an increase in the linear depolarization ratio (L_{DR}) and applications to hail identification are presented in [11], [12], [13], [14]. The decrease in the co-polar correlation coefficient ρ_{hv} is the fourth polarimetric characteristic of hail [15], [16]. In [17] Ryzhkov et al. use a one-dimensional hail model that can generate any realistic size as hailstones are introduced in the updraft where they grow. The shape, however, is an imposed spheroid with a specified axis ratio. To our knowledge, there are no models that can generate protuberances. In principle, this could be done empirically, as there is no theory to relate protuberances to hail size and its thermodynamic environment.

This paper is aimed at systematically representing the results of rough hailstones that multiple publications (i.e. [17], [16], [18], etc.) find most likely to cause low ρ_{hv} and extreme Z_{DR} observations. While Jiang et al. [18] make a significant step in modeling realistic hailstones, their database is limited to eight hailstones. Thus it cannot represent corresponding polarimetric signatures. Herein, we focus on S-band (WSR 88D's frequency band) and create the database of spheroidal rough hailstones

Funding was provided by NOAA/Office of Oceanic and Atmospheric Research under NOAA-University of Oklahoma Cooperative Agreement #NA16OAR4320072, U.S. Department of Commerce

Dj. Mirkovic is affiliated with Cooperative Institute for Mesoscale Meteorological Studies, The University of Oklahoma, and NOAA/OAR National Severe Storms Laboratory, Norman, OK 73072 (e-mail: Djordje.Mirkovic@noaa.gov).

D. S. Zrnic is affiliated with NOAA/OAR National Severe Storms Laboratory, and School of Meteorology, and School of Electrical and Computer Engineering, University of Oklahoma, Norman, OK 73072 (e-mail: Dusan.Zrnic@noaa.gov).

V. Melnikov is affiliated with Cooperative Institute for Mesoscale Meteorological Studies, The University of Oklahoma, and NOAA/OAR National Severe Storms Laboratory, Norman, OK 73072 (e-mail: Valery.Melnikov@noaa.gov).

P. Zhang is affiliated with Cooperative Institute for Mesoscale Meteorological Studies, The University of Oklahoma, and NOAA/OAR National Severe Storms Laboratory, Norman, OK 73072 (e-mail: Pengfei.Zhang@noaa.gov).

covering most naturally observed hailstone sizes. This paper is primarily concerned with the Z_{DR} and ρ_{hv} because these two variables may discriminate some hail sizes. For example, a dry hail model [19] consisting of oblate spheroids produces negative Z_{DR} up to – 6 dB at sizes larger than 30 mm at S-band. Therefore, these authors propose that negative Z_{DR} might indicate the presence of large dry hailstones. The negative Z_{DR} is caused by resonance and occurs at different sizes depending on the frequency band [17]. Balakrishnan and Zrnic [15] speculate that negative Z_{DR} indicates wet oblate hail with a maximum dimension larger than 40 mm. According to the computations in [20], spongy oblate hail can have large positive or negative Z_{DR} (depending on the fraction of water in the hailstone) in a size range of approximately 30 to 60 mm.

The decrease of ρ_{hv} has been connected, albeit indirectly, with hail size as follows. Large hail is prone to be either oblate or irregular, both exhibiting protuberances and tumbling. These effects decrease ρ_{hv}. Quantifying the Z_{DR} and ρ_{hv} for hail sizing is ongoing research, and it is unlikely that the two stand-alone would do. This is why [14] chose to estimate size from the polarimetric variables' vertical profiles below the melting layer.

We chose to model oblate hail with protuberances. In the next section, we explain the reasons for this choice. We present our findings as follows. First, we overview hailstone models and electromagnetic (EM) modeling procedures. In section three, we describe our approach to calculating polarimetric variables and our hailstone models' results. We consider some hailstorm observations in section four and use our results to interpret data and discriminate hail size. And finally, we revisit our findings and stress important details.

II. Hail, physical properties, and impact on models

We discuss the polarimetric variables' values from hail at the S-band and relate these to some hail models.

A. Polarimetric properties

Unlike raindrops, hailstones' size and shape are not uniquely related. Nonetheless, it is known that small hail (< 10 mm) is generally spherical, whereas larger stones have a variety of shapes and the oblate one occurs more often. This has important ramifications on detection and estimation of size. Among the first study documenting hailstone shapes (in America and Europe) is by Weikmann [21], who found that 58% had a spheroidal shape, and of these, 68% were noticeably oblate. Browning and Beimers [22], writing about Oklahoma hail, state "the majority of hailstones were only very slightly oblate when they were 10 mm in diameter, but most became markedly oblate by the combined effects of growth and melting." Barge and Isaac [7] observed 83% of hail with axis ratios between 0.6 and 1. Mean axes ratios 0.6 to unity are reported in [23], [24]. Giammanco [25] plotted minimum to maximum dimension ratios over two years for the Great Planes hail. The values are consistent with [23].

Moreover, one standard deviation on either side of the mean encompasses the mean values measured in hail from Oklahoma, Alberta, and Colorado [23]. One of us (Dusan) had experienced several hailstorms in Oklahoma. On a few occasions, he saw disk-shaped hailstones with maximum sizes of 40 to 60 mm. In Fig. 1 are three hailstones from Oklahoma with oblate shapes, the largest dimension of about 50 mm, and some protuberances along the perimeter. This motivates our choice to model hail as an oblate spheroid, but with the following caveats. The significantly oblate hailstones span a relatively narrow range of sizes, and these appear to be at the transition from large to giant hail, perhaps 40 to 60 mm? Other very irregular shapes are important and often dominate in the giant hail category.

B. Models

The physical properties for determining scattering from hail are the shape, size, and refractive index. Often the assumed shape is spheroidal [17], [13], [26], and the refractive index can be of pure ice, water coated ice, or spongy ice [20].

One of the main challenges for models is reproducing the observed low ρ_{hv} [17]. The low correlation coefficient values are most likely caused by the irregular shape of hailstones aloft [16]. Balakrishnan and Zrnic [15] considered surface protuberances and quantified the decrease of the ρ_{hv} as a function of protuberance to diameter ratio. Their model applies the Rayleigh solution to sizes for which the approximation begins to break down. Therefore, their results may serve as a rough guideline for non-Rayleigh scatterers. Jiang [18] computed the polarimetric variables using models based on eight hailstones collected in nature. Five of these were smaller than 40 mm, and three were larger than 100 mm. The authors made three-dimensional scans of collected hailstones and created numerical models to simulate their polarimetric signature. They used the Discrete Dipole Approximation (DDA) scattering technique in the simulation of scattered fields. Their results exhibit a significant decrease in ρ_{hv} for some of the modeled "wet" hailstones. However, the authors use a fixed 1 mm water coating, which is applicable to a narrow band of sizes centered at about 60 mm. Their models of hailstones 10 to 70 mm in size show no significant decrease in ρ_{hv}. Jiang et al. [18] also compare the backscatter differential phase δ of spheroids with their model results. They use only four water-coated hailstones due to the numerical complexity of the DDA in such cases. The results they present are important because δ exhibits significantly larger variation (about 100°) compared to the calculated ones with forward operator assuming spheroidal shape of hailstones [17].

C. The Model

Here we present a spheroid-based scattering model of hail with surface protuberances. Following [15], the model differentiates hailstone types according to the axis ratio of an initial oblate spheroid, protuberance to radius ratio, and hailstone size. The maximum dimension determines the hailstone size. In the case of an oblate spheroid, this is the equatorial diameter. We opted for the maximum dimension instead of the often used equivolume diameter because the maximum dimension is measured in field experiments when hailstones are collected. Our models include dry and water-coated ("wet") hailstones with axis ratios 0.6 to 0.8 and sizes up to 100 mm. Scattering coefficients obtained by each hailstone

model's simulations are stored in a library of scattering matrices containing about 1000 different spheroidal rough hail models.

For dry hail, spheroids have a solid ice refractive index, whereas, for wet hail, spheroids consist of two layers. Protuberances are added to the surface of the hailstone randomly. Quantifying the surface roughness is challenging because the relation to the diameter is not known. To overcome this challenge, we evaluated images of hailstones from April 21, storm available online [27], [28], [29]. In these videos, the authors collected hailstones for which we roughly evaluated roughness to diameter relation (Fig. 1 b). We define roughness as protuberance's maximal deviation from the original (starting) spheroid's equatorial radius. Hailstones from the April 21 storm (Fig. 1 a) have protuberances of about 20% of the diameter. Following our rough approximations, we modeled hailstones with 2%, 6%, 10%, and 14% roughness.

Water content for wet hail was determined using the maximum surface water amount before shedding, as suggested by [30]. The water content is uniformly distributed over the hailstone's surface, following its shape (topography). This assumption may not replicate the true distribution of water on hailstone, yet it may be a reasonable approximation. For oriented hailstone, we expect water to shed off of the perimeter and backside. In contrast, a tumbling hailstone would accumulate and shed water in the plane to which the rotation axis is perpendicular.

D. Computational Electromagnetic (CEM) solvers

Electromagnetic (EM) modeling of hailstones was done using the commercially available software WIPL-D Pro [31]. It uses the Method of Moments (MoM) computational EM tool designed to analyze 3D metallic and dielectric structures. A hailstone is represented as an object composed of interconnected plates that define a boundary between two different materials. An appropriate refractive index is assigned to the inner and the outer medium setting boundary conditions. From the incident electric field and boundary conditions for both the electric and magnetic field, the matrix of equivalent induced surface currents can be computed. Equivalent induced currents are determined for each surface element and approximated by a product of unknown coefficient and higher-order polynomial basis function. The matrix system is solved to determine the "unknown" coefficients. These coefficients with the basis function are then used to determine the hailstone's scattered EM field.

MoM and WIPL-D have been validated on many man-made objects [32], as well as insects and biota [33] [34]. MoM has been previously used for computational EM (CEM) calculations of scattering by hydrometeors. Some early works include modeling hail [35], [36], while some of the latest meteorological applications include the prediction of scattering by 3D snowflakes [37].

Various investigators have applied different CEM approaches to hydrometeor scattering. Most common is the T-matrix method, but many recent studies employed the DDA. The full-wave solvers were mainly applied to validate results and for accuracy/computation speed comparisons. Several publications exist where these CEM approaches are compared [38], [39], [40], [37]. Some only validate the accuracy of CEM using MoM (WIPL-D) against other solvers [40]. A comparison of the MoM-surface integral equation (MoM-SIE) approach (which is used in WIPL-D) is the topic in [38] and [37]. The authors [40], [39], [37] examine the T-matrix method's stability in different scenarios. For example, [40] studies the stability at a fixed frequency while varying the axis ratio, whereas [37] and [38] use the frequency variation. Of particular significance are comparisons of DDA with MoM-SIE regarding the computational intensity of calculations. MoM-SIE is, on average, more accurate and two orders of magnitude faster than the DDA and is more versatile than the T-matrix method [39].

III. CALCULATION OF POLARIMETRIC VARIABLES

Forward operators [41] use scattering coefficients for the principal axes of a spheroid (normal incidence) obtained via Rayleigh or some other (T-matrix) method. Normal incidence signifies the particle is not canting. Away from normal incidence, researchers rely on the "backscattering rule," a closed-form approximation of backscattering matrix, to extrapolate the scattering coefficients. This extrapolation holds up to 10° away from normal incidence measured from the symmetry axis of spheroidal raindrops (Rayleigh scatterers) and frequencies to 35 GHz [42]. However, when applied to hail, the backscattering rule must accommodate tumbling hailstones, which creates a significantly larger angle between the incident electric fields and the scatterer's symmetry axis. Therefore, using the backscattering rule out of its valid angular range would introduce errors to calculations of the polarimetric variables at resonant and larger hail sizes [40]. To further examine the angular moments' application and the backscattering rule reader can look in [43].

The accurate alternative is determining the scattering coefficients for all canting and orientation angles and avoiding the backscattering rule out of its valid range. Such an approach is most appropriate for non-symmetrical hydrometeors. Here, we use the definition of canting in the plane of polarization and orientation from the direction of propagation (Fig. 1) in Ryzhkov [43].

The variability of scattering coefficients for non-symmetric hailstones is naturally larger compared to symmetric ones. Whereas radially symmetric objects have independent scattering coefficients over a single arc of 90°, a truly non-symmetric model with random protrusions may scatter differently for each canting angle.

Here, we adopt a direct approach to calculate the scattering coefficients for various user-defined canting and orientation angles (α, ψ). Polarimetric variables are computed from scattering coefficients as:

$$Z_{\mathrm{h}} = \frac{4\lambda^4}{\pi^4 |K_{\mathrm{w}}|^2} \sum_{\mathrm{i}}^{N} N_{\mathrm{Di}} \sum_{\Omega} |s_{\mathrm{hh}}|^2 \quad \left[\frac{\mathrm{mm}^6}{\mathrm{m}^3}\right] \tag{1}$$

$$Z_{\mathrm{H}} = 10 \log Z_{\mathrm{h}} \ [\mathrm{dBZ}]; \tag{2}$$

$$Z_{\mathrm{v}} = \frac{4\lambda^4}{\pi^4 |K_{\mathrm{w}}|^2} \sum_{\mathrm{i}}^{N} N_{\mathrm{Di}} \sum_{\Omega} |s_{\mathrm{vv}}|^2 \quad \left[\frac{\mathrm{mm}^6}{\mathrm{m}^3}\right]; \tag{3}$$

$$Z_{\mathrm{DR}} = 10 \log \left(\frac{Z_{\mathrm{h}}}{Z_{\mathrm{v}}}\right) \ [\mathrm{dB}]; \tag{4}$$

$$|\rho_{\rm hv}| = \frac{|\sum_i^N N_{\rm Di}\Sigma_\Omega\langle s_{\rm hh}^* s_{\rm vv}\rangle|}{\sqrt{\sum_{\rm i}^{\rm N} N_{\rm Di}\Sigma_\Omega|s_{\rm hh}|^2}\sqrt{\sum_{\rm i}^{\rm N} N_{\rm Di}\Sigma_\Omega|s_{\rm vv}|^2}}; \quad (5)$$

$$\delta = \arg(\rho_{\rm hv}) \ [\rm deg]; \quad (6)$$

$$L_{\rm DR} = 10\cdot\log_{10}\left(\frac{\sum_i^N N_{\rm Di}\Sigma_\Omega|s_{\rm hv}|^2}{\sum_{\rm i}^N N_{\rm Di}\Sigma_\Omega|s_{\rm hh}|^2}\right)[\rm dB]\ ; \quad (7)$$

$$C_{\rm DRa} = 10\cdot \log_{10}\left(\frac{\sum_{\rm i}^N N_{Di}\Sigma_\Omega|s_{\rm hh}|^2+\sum_{\rm i}^N N_{Di}\Sigma_\Omega|s_{\rm vv}|^2-2Re\left\{\sum_{\rm i}^N N_{\rm Di}\Sigma_\Omega\langle s_{\rm hh}^* s_{\rm vv}\rangle\right\}}{\sum_{\rm i}^N N_{Di}\Sigma_\Omega|s_{\rm hh}|^2+\sum_{\rm i}^N N_{Di}\Sigma_\Omega|s_{\rm vv}|^2+2Re\left\{\sum_{\rm i}^N N_{\rm Di}\Sigma_\Omega\langle s_{\rm hh}^* s_{\rm vv}\rangle\right\}}\right)[\rm dB], \quad (8)$$

where $s_{\rm xy}$ are the scattering coefficients, α is the canting angle, $N_{\rm Di}$ is the concentration of each hydrometeor, $|K_{\rm w}|^2$ is the dielectric factor (0.93 here), i represents the summation index over hydrometeors in the unit volume, whereas summation over $\Omega = (\alpha, \psi)$ are various orientations in a unit volume. The wavelength λ in our computations is 107 mm. The simulated polarimetric variables represent the ones measured in the alternate polarimetric mode, whereby the H and V polarized pulses of EM radiation are sent separately. This follows the approach set by [17] [18]. Nonetheless, for mean canting angles of 0°, as considered herein, the polarimetric variables measured in the alternate polarimetric mode and simultaneous mode (as on the WSR-88D) are almost the same.

The Circular depolarization ratio ($C_{\rm DRa}$) we use is obtained from linear polarization returns [44], [45], [46] hence is a proxy of the true $C_{\rm DR}$. We resort to this proxy, as it can be obtained from the WSR-88D data. Appendix A details the differences between the true $C_{\rm DR}$ and the simulated (proxy) $C_{\rm DRa}$.

IV. Polarimetric variables in hail, model results

Our results are presented assuming a monodispersed size distribution as in [17]. We calculate the polarimetric variables for various orientation angles ψ and canting angles α. The canting in plane of polarization α changes from 0° to 40°, with the mean canting angle being 0°. The monodisperse size distribution is used to stress the scattering difference between hailstone sizes and compute the polarimetric variables at each size. This way, one can quickly determine the sizes that cause the most significant changes in the polarimetric variables; or the sizes at which some polarimetric variables cross a threshold. This is important as it offers a solution to the inverse problem, that is, from observed polarimetric variables, find the dominant contributing sizes. Hail has a highly variable distribution of sizes which smooths the polarimetric variables, thus blurring the separation of sizes. Nonetheless, in cases, as herein, where a small range of sizes causes a significant difference in any of the polarimetric variables, the monodisperse simulations enable identifying the range of sizes that the distribution has blurred. The added complications come from the highly variable refractive index of hail, and that is why we distinguish dry hail and wet hail.

Hailstone orientation is introduced in the CEM modeling, where the direction of incident fields is varied to assume particle tumbling, as in [18]. Our hailstone model, in simulation, has its equatorial plane in *x*O*z* plane, which allows for the implicit introduction of hail canting. Changing the spherical coordinates of incident EM field $(\varphi, \theta)\epsilon[(0,2\pi),(-\pi,\pi)]$ therefore translates to change of hail orientation and canting (α, ψ). This is different if compared to Jiang et al. [18], where the models' equatorial plane is in x*Oy* plane and canting in the plane of polarization (α) is introduced through rotation of fields in the polarimetric variable calculation.

We calculate polarimetric variables for hail sizes of 5 mm to 100 mm in steps of 5 mm. The values between points are interpolated using a modified Akima algorithm [47]. Sizes are based upon the fact that hailstones smaller than 8 mm would typically melt in fall [17], while sizes exceeding 100 mm are very uncommon. Nevertheless, our approach applies to both smaller and larger sizes.

A. Dependence on the axis ratio

Consider how axis ratios of hydrometeors having 2% surface roughness affect the polarimetric variables. The results for hailstones with low roughness should resemble perfect spheroids published in [17].

As we use the maximum diameter instead of equivolume diameter, the first resonance in radar reflectivity factor (Fig. 2 *a*) occurs at noticeably different sizes for various axis ratios. This difference is expected as the axis ratio is different for each of the curves. If we were to use equivolume diameter, these would be closer to each other at resonance.

Resonance characteristics are observed in all polarimetric variables at horizontal and vertical polarization (Fig. 2). The polarimetric variables at horizontal polarization for dry hail are plotted in Fig. 2 *a*); the first resonance peak, the second, and the third are easily distinguished. Identifying major resonances for wet hail (Fig. 2 *b*) is easier because the two maxima are well pronounced. The internal H electric fields in scatterers add constructively, or destructively, at different sizes than V fields. These differences affect the polarization variables causing visible effects on $Z_{\rm DR}$, $\rho_{\rm hv}$ and δ. We see some effects also on the $L_{\rm DR}$ and $C_{\rm DRa}$ yet these are not as pronounced.

The $Z_{\rm DR}$ in dry hail becomes negative starting at sizes 60 to 70 mm (depending on the axis ratio) and remains negative up to the end of the simulated maximum size (100 mm) (Fig. 2 *c*). This characteristic may have strong implications for giant hail discrimination in the dry hail regions. Dry hail contrasts to the wet hail model with negative $Z_{\rm DR}$ at sizes between 45 and 70 mm. The results are in qualitative accord with [15], their Fig. 6 *b*) in which, for comparison, the sign of the $Z_{\rm DR}$ should be reversed because the minor axis is in the horizontal plane; the values in Figs. 2 *c*), and *d*), are about two times more negative than in [15]. This may be because these authors' model assumes spheroids with the symmetry axis randomly oriented in the plane along the beam and normal to the ground. This effectively reduces oblateness. Similar is the comparison with the model [17]. The radar reflectivity factor Figs. 2 *a*), and *b*) and Figs. 8 *a*), and *b*) in [17] follow the same pattern as for our 0.8 axis ratio hailstones. Yet, there are some discrepancies in the $Z_{\rm DR}$ (Fig. 2 *d*) and those in [17] Fig. 8 *d*). The main difference is the positive $Z_{\rm DR}$ maximum in [17] observed at 8 mm, whereas our results do not have it. The reason for this difference is in the physical model of hailstones. Here we use the maximum water prior to shedding as water coating of solid ice, while in [17] it is based on the hail water fraction. An 8 mm size particle in [17] is pure water, whereas for slightly larger sizes, it is spongy hail containing water within the hail core, contrary to our solid ice

core model. In our simulations, 5 mm hailstone has an ice core of 5 mm and water coating surrounding it. Water within the hail core in spongy hail models will increase the ice core's dielectric permittivity, making it higher than the permittivity of solid ice. Furthermore, the high Z_{DR} (>5 dB for 0.6 axis ratio) of wet hailstones from 20 to 35 mm in size (Fig. 2 *b*) may explain large Z_{DR} values in severe convective storms observed by [48]. Others claim that such large Z_{DR} "cannot be reproduced in scattering calculations or forward operators employing liquid-coated spheroids" [18].

Notice in dry hail's ρ_{hv} the significant drop is at the axis ratio of 0.6 and sizes 85 to 90 mm (corresponding to equivolume diameters of 78 to 82 mm. These are about 40% larger than reported in [15]. For sizes up to 60 mm, results in [15] (their Fig. 6 *a*) and our results agree well with the ρ_{hv} decreasing to about 0.98.

Wet hail significantly increases drops in $\rho_{hv.}$ Sizes at which decrease occurs depend on the axis ratio. The first decrease happens at 60 mm (equivalent diameter of 55.7 mm); for the axis ratio of 0.8 (Fig. 2 *f*), it produces ρ_{hv} = 0.83. This result corroborates Fig. 10 *a)* in [15]. Some discrepancy is observed in the modeling of 0.6 axis ratio wet hail. For sizes up to 10 mm, Balakrishnan and Zrnic [15] (in their Fig. 10 *a*) find local ρ_{hv} minimum (about 0.94), which doesn't exist in our results. This discrepancy is most likely due to different modeling of hailstones.

Sizes of about 95 mm and 100 mm (and more not shown) cause decreases of ρ_{hv} to 0.75 (for 0.7 axis ratio) and 0.7 (for 0.6 axis ratio) as depicted in Fig. 2 *f*). Note that ρ_{hv}=0.85 is the lowest admissible value for hail classification [26]. The observed low values come from a distribution of hail sizes. And we alert readers that in the case of different sizes and axis ratios, the composite ρ_{hv} is between the smallest and largest one of the bunch.

The backscatter differential phase δ (Fig. 2 *g* and Fig. 2 *h*) exhibits wide changes. These changes are, to a larger extent, responsible for the decrease of ρ_{hv}. Note that Jiang et al. [18] (their Fig. 11) have a smaller range of δ for the same canting angles.

L_{DR} and C_{DRa} are increasing in the dry hail for all axis ratios in Fig. 2 *i*), Fig. 2 *l*). Researchers [49] and [18] recognized this trend as a potential tool for hailstone size determination. Interestingly, the L_{DR} of dry hailstones deviates from general trend substantially only for some resonant sizes of very rough hailstones (14%) (Fig. 3 *e*). While for hailstones with smaller protuberances L_{DR} increase with size up to about 80 mm.

The L_{DR} measurements cannot be made on the current WSR-88Ds. Because of L_{DR}'s dependence on the particle's shape and orientation, C_{DRa} is deemed advantageous over L_{DR} [45]. General increase of C_{DRa} suggests that it might be useful for hailstone size detection above the melting layer and regions where dry hail is the main contributor to scattering. The C_{DRa} is mainly dependent on the axis ratio and size, while its dependence on surface roughness is insignificant (Fig. 2. *l*). Furthermore, C_{DRa} is at least 5 dB higher than the linear depolarization ratio [45]. However, once wet hail reaches resonant size (60 mm maximum or 55.5 mm equivalent volume diameter), the variation of the C_{DRa} becomes very pronounced (Fig. 2 *l*), similar to the variation of the L_{DR} (Fig. 2 *j*).

B. Dependence on the surface protuberance

Comprehensive studies quantifying the effect of surface roughness on all polarimetric variables have yet to be made. Some attempts to quantify the surface roughness effect on one or a few variables exist [15]; [18]. Jiang et al. [18] analyze eight actual hailstones and compute the polarimetric variables therefrom. Although limited, it is significant that their correlation coefficient from the largest hailstone exhibits changes between 0.82 (standard deviation of canting angle was 10°) to 0.56 (at a standard deviation of more than 60°).

This section considers dry and wet hailstone models with a 0.7 axis ratio and roughness of 2%, 6%, 10%, and 14% (Fig. 3). Reference [40] includes hailstones with the same protuberances but axis ratios of 0.6 and 0.8.

Balakrishnan and Zrnic [15] consider the effect of surface protuberance on ρ_{hv} for spherical Rayleigh scatterers. Their results of the ρ_{hv} decrease for distorted spheres can be used for quantitative comparisons with our computed decrease in dry hail. However, a similar comparison in the wet hail case would be off, mainly because differential phases are neglected in Rayleigh scattering. Due to their water coating, these scatterers have a higher backscatter differential phase than dry hailstones (compare 20 to 60 mm Fig. 3 *g*) and Fig. 3 *h*)). Results in Fig. 7 of [15] show a continuous decrease in the ρ_{hv} with increasing protuberance to diameter ratio. This result is independent of hail size.

The correlation coefficient (Fig. 3 *e*) depends on roughness only for resonant sizes (50 to 60 mm and 80 to 100 mm). In contrast, no significant dependence on roughness is observed for other sizes. Mirkovic [40] in his Figs. 8.21 & 8.22 observes a drop in correlation coefficient for dry hailstones of about 15 mm with a 0.6 axis ratio in accord with maximal ρ_{hv} drop predicted by [15]. Herein, if we consider the drop of the ρ_{hv} for 90 mm dry hail with 14% roughness (ρ_{hv}=0.87) (Fig. 3 *e*), and compare it to the 2% roughness (ρ_{hv}=0.96) (which we consider smooth), we see that the drop agrees with [15]. Similar applies to other roughness at resonances, yet minimal values are not significantly different from one another except for the 14% protuberances. Our computed values for dry hailstones are in accord with [18] Fig. 7 for all hailstones they have modeled.

If we consider wet hail (Fig. 3 *f*)), the drop in the ρ_{hv} becomes significantly larger and aligned with change in the backscattered differential phase (at about 55 mm size). Whereas, for resonant hailstones with smaller roughness the ρ_{hv} remains between 0.85 and 0.9; the ρ_{hv} for resonant hailstones with 14% roughness ρ_{hv} drops to 0.3. Similar dependence is observed in hailstones with 0.6 and 0.8 axis ratios having 10% and 14% roughness. This result is important considering that recent models fail to replicate observed low ρ_{hv} in wet hailstones and reach the minimum of 0.88 (Fig. 7 a) in [50]); minimum of 0.97 (Fig. 7 S-band correlation coefficient) in [41]; 0.6 for "hailstone 4" in Fig. 12 by [18]. Furthermore, it suggests that including surface protuberances may be necessary for the realistic modeling of hailstorm signatures.

Jiang et al. [18] is the most recent study considering the L_{DR} of wet hailstones with irregular shapes. They simulated four wet hailstones and their highest simulated L_{DR} is about -8 dB and the corresponding hailstone looks like a "rabbit head."

Examining the information available, namely Z_{DR}(Fig. 5 in [24]) for this hailstone with no canting, we can approximate its oblateness. It follows that the axis ratio is about 0.4, which is significantly more oblate than the values we simulated. Nevertheless, our result has the same order of magnitude, i.e., L_{DR}= -13 dB for a wet 0.6 axis ratio hailstone similar in size (about 30 mm).

Presented signatures of L_{DR} and C_{DRa} dependence on hailstones' roughness favors the circular depolarization ratio for its linearity in dry hail. The dry hail size discrimination proposed by [45] depends on the linearity of the C_{DRa}, and quasi linearity is maintained up to 80 mm hail. Except for very rough (14%) hail at its resonance (at about 60 mm) the C_{DRa} remains mostly linear (Fig. 3*k*), whereas L_{DR} has stronger dependence on surface roughness. Therefore, C_{DRa} may be better suited for dry hail size discrimination [45].

V. Polarimetric Variables in Hail, Observations

Present knowledge about hail size distribution (HSD), shape, and orientation in fall is scant. Various shapes have been observed on the ground, and the large ones can be extrapolated to locations aloft. A comprehensive summary of hailstone and graupel polarimetric attributes is in [6]. Herein we present observations of a hailstorm from opposite directions by two WSR-88D weather radars. Both radars measure significant negative Z_{DR} in the common area, and we discuss these after reviewing possible causes.

Shape and orientation are weakly related to size. Our results and others suggest the following possibilities:

1) *Small graupel (< 5 mm), when its shape is conical, is vertically oriented. Observations include consistently negative Z_{DR} (-0.5 to -0.2 dB) and Z smaller than 40 dBZ [51].*
2) *Oblate wet hail (10 to about 40 mm), if oriented with symmetry axis in the horizontal plane, will create negative Z_{DR} as reported, for example, in [24], [15]. Such hail may spin about its symmetry axis [52].*
3) *Oblate horizontally oriented wet hail with size 40 to about 60 mm will cause negative Z_{DR} (Fig. 2 d) and [24], [15].*
4) *Differential attenuation can induce negative Z_{DR} [53], [16].*

Negative Z_{DR} cannot be obtained by assuming exponential or uniform HSD. If we examine the results for wet hail in Fig. 2 and 3 *d*), we see that only sizes between 45 and 65 mm (resonant sizes) produce differential reflectivity below -1 dB. Therefore, to achieve negative Z_{DR}, resonant sizes would have to be dominant contributors. To quantify, let us consider two-step HSD. Let the first step be from 25 to 40 mm, having concentration *a,* and the second step from 45 to 70 mm, of concentration *b*. For a fixed concentration (say b=1) of resonant size (45 to 70 mm) hail, the concentration of smaller sizes to achieve $Z_{\mathrm{DR}} = -1.5$ dB has to be $a \leq \frac{2}{27}$ otherwise, Z_{DR} would be larger than -1.5 dB. We have assumed the 0.7 axis ratio and small (2%) protuberance. For different axis ratios or protuberance levels, this result may vary slightly. Following this example, we can conclude that HSD must be narrowly centered at 50 to 60 mm (center of resonant sizes) to produce the relatively small negative Z_{DR}.

For the case that we present, data were collected during the April 22 hail storm in South-West Oklahoma by the KTLX, and KFDR, WSR-88Ds over Comanche county, OK. The storm produced large 44.5 mm (1.75in) and giant 50 mm to 76.2 mm (2 to 3 in) hail in Fletcher, OK [54]. The largest hail reported in Fletcher, OK, was at 4:11 UTC when 76.2 mm (3 in) hail occurred. The Norman Weather Forecast Office (OUN) reported the 76.2 mm hail at 4:11 UTC in Elgin, OK, [55]. Which would be within the same hail core, as these two cities are within the circle (Fig.4). Additionally, a group of storm chasers documented sizes and shapes of hailstones in their videos [27] [29] [28]. In these videos, hailstones were compared to baseballs [28], collected and compared against hand palm [27] (Fig. 1 a), and gauged by Vernier calipers [29]. Validation of our hypothesis on hail size aloft is next to impossible. However, relating to the ground observation of hailstones at multiple locations from multiple sources yields results that agree with our hypothesis. The majority of collected hailstones are about 50 mm in diameter, with the occurrence of hailstones up to 75 mm.

The Hail Detection Algorithm (HDA) on the WSR-88D identified this region as giant hail. We examine reflectivity (Z), differential reflectivity (Z_{DR}), and correlation coefficient (ρ_{hv}) fields from KTLX and KFDR radar. It is important to note that these radars operate at 2.91 GHz (KTLX) and 2.71 GHz (KFDR), which are on the low and high side of the frequency spectrum (2.7-3GHz) reserved for the WSR-88D. Only a few radars operate above 2.9 GHz. The frequency in our hailstone simulations is in the middle of this range at 2.8 GHz.

The storm center is at about 84 km from the KFDR and about 107 km from the KTLX. The lateral dimension of the KFDR's beam at 0.9° elevation is completely within the KTLX's beam's lateral dimension at 0.5° elevation. As these beams cover the same area, additional information may be extracted from the Z_{DR} signature. Because the resonance position depends on the wavelength, the size at which KTLX observes negative Z_{DR} is about 7% smaller than in the KFDR case. The frequency difference may contribute to the observed Z_{DR} differences.

In Fig. 4 are the fields of polarimetric variables collected with the KTLX radar. Additional observations include video reports from individuals on video-sharing websites [28].

We have circled the region of interest for our example. Within the circle is the observation of the hail core with radar reflectivity higher than 60 dBZ, predominantly negative Z_{DR}, the correlation coefficient of about 0.6 to 0.95, and a "valley" (15° to 45°) in differential phase between two "ridges." We calibrated Z_{DR} by removing the bias, the Radar Operation Center estimates from Bragg scattering [56]. The reported bias for that day is -0.32 dB. The lowest Z_{DR} within the region is -3.14 dB. By applying the algorithm of Ryzhkov et al. [16] for KTLX radar within the circle (Fig. 4) we calculate the average differential attenuation of 0.07 dB (°)$^{-1}$ or 2.59 dB for an average $\Delta\Phi_{\mathrm{DP}}$ of 37°. The differential reflection after both corrections are applied is -0.55 dB, and thus noit increases the Z_{DR}, it leaves a coherent patch in the circled area.

Similar to the observations by the KTLX are the observations of the same hailstorm by the KFDR (Fig. 5). The view is from the opposite direction, and that helps solidify some conclusions. We have removed the bias in Z_{DR} of -0.19 dB from these data.

Again we see the region of consistently low Z_{DR}but now, with a minimum of -2.17 dB. We calculate the average differential attenuation in the circled region of KFDR (Fig. 5) as in [16] to be 0.02 dB $(^o)^{-1}$ or 0.51 dB for an average $\Delta\Phi_{DP}$ of 26.5°. After both corrections are applied, the differential reflectivity is -1.66 dB. The Φ_{DP} field in Fig. 5 is consistent with the one in Fig. 4. It exhibits a similar "valley" between ridges of high differential phase with a change of about 30°. However, due to the difference in radar position with respect to the storm, the differential attenuation differs by 2.08 dB. In our case, Z_{DR} miscalibration and differential attenuation that we correct would be the main sources of error. The hail core size is multiple beamwidths wide, and thus non-uniform beam filling effects and the difference in the observation time of these radar beams for the two radars are not present.

The remaining Z_{DR} the difference might be caused by the radars' operating frequencies. For example, if the distribution of sizes favors the resonant one for the KTLX, the corresponding number of negative Z_{DR}s would be larger and vice versa. The area of common negative Z_{DR} delineated with the circle in Fig. 6, we believe is due to large oriented oblate hail.

Some observations of negative differential reflectivity in literature are in [57]. The authors report $Z_{DR} \sim -2$ dB with associated reflectivity of 65 dBZ above the melting layer. The values and location of the signature are consistent with the wet growth of giant hail. Based on our results, we can associate this region with resonant size hail.

Another example is in Fig. 7 of [12], which shows results obtained by the NCAR's S-pol radar. It indicates a region of large hail aloft with a reflectivity of about 60 dBZ, $Z_{DR} = -1.5$ dB, and $L_{DR} = -12$ dB. This signature corroborates well with our calculations of resonant size hail for all three variables.

VI. Discussion and Conclusions

We have systematically examined and quantified the effects of irregular hail shape on the polarimetric variables. As in numerous previous studies, the underlying physical model is the oblate spheroid, to which we have added protuberances. There are no comprehensive studies of such models, likely due to the complexity of scattering from rough bodies. This motivated us to choose the commercially available electromagnetic solver WIPL-D Pro for calculating the scattering coefficients. Commercially available solvers make easier replication of similar studies than would be possible with proprietary tools. Moreover, EM solvers are more versatile than specialized techniques and have documented accuracies. Because customer needs drive development, EM software are continually optimized to achieve faster and more accurate performance; this makes them desirable for modeling scatter off hydrometeors.

Surface roughness, commonly observed on dry and wet hailstones, can significantly change the hailstones' radar cross-sections (RCS) compared to RCSs of spheroids. However, for most sizes, surface protuberances cause insignificant change to the reflectivity factor Z_h. Significant variations in Z_h occur for resonant size (45 to 60 mm) and extremely large wet hydrometeors.

Differential reflectivity can be significantly affected by protuberances. We observe a large decrease (>6dB) for very rough resonant size hailstones. Negative (<-2dB), as well as large positive values (>5dB) of Z_{DR} have been reported and replicated with different monodispersed models. Besides the large negative Z_{DR} drop for 0.7 axis ratio hailstones, a similar increase in Z_{DR} occurs for 30 mm wet hailstones with 10% and 14% protuberances. The capability to simulate these observed signatures is one important outcome of our approach.

The co-polar correlation coefficient is arguably one of the most important polarimetric variables for determining hail aloft. Calculation of ρ_{hv} using only spheroidal models has significant limitations because the computed scattering coefficients are independent only over a 90° arc. Because it is a measure of the correlation between the horizontal and vertical return, ρ_{hv} is quite sensitive to the axis ratio as well as protuberance levels. Results presented herein quantify this sensitivity. It is important to note the large ρ_{hv} drop (to 0.3) for the very rough 0.7 axis ratio wet hailstone. A similar drop occurs for the 0.6 axis ratio hailstones with the same roughness levels. These low ρ_{hv} are important as they may cause misclassification of hydrometeor type; hydrometeor classification algorithms associate low ρ_{hv} with non-meteorological scatterers.

Our results confirm that use of L_{DR} as well as C_{DRa} for hailstone sizing is plausible. Both variables deviate significantly from a monotonic change at a 14% roughness for 0.6 axis ration. A problem in the application of L_{DR} and C_{DRa} to size discrimination of dry hail is their dependence on the hailstone axis ratio. For example, both variables exhibit about 7 dB difference between the values at axis ratios of 0.6 and 0.8. Our dry hail model with a size larger than 65 mm produces negative Z_{DR} whereas, for wet hail, the sizes of 45 to 70 mm cause negative Z_{DR}. It remains to be seen if similar relations hold in nature. If true, the relations could be useful for discriminating dry from wet hail and recognizing the giant hail category.

We presented fields of the polarimetric variables from a severe hailstorm in which significant negative Z_{DR} were recorded by two WSR-88D viewing the storm from opposite directions. We hypothesize that the main contributors to the commonly observed negative Z_{DR} are oriented wet hailstones in size range 45 to 70 mm. The observed values are less negative than the simulated ones. This is not surprising because the simulated results apply to the alternate polarimetric mode and hence yield larger extreme Z_{DR} of either sign. In the simultaneous polarimetric mode, the variations of the canting angle tend to reduce the extreme Z_{DR}s. Differential attenuation, however, causes negative Z_{DR} bias.

Appendix

A. Circular Depolarization Ratio and its proxy

A brief description of what C_{DR} we measure and simulate is given here to avoid possible confusion between models and observations. This is to reconcile the values used in this manuscript with the true and proxy values.

1) Exact C_{DR}

By definition, the C_{DR} can be computed from the linear H, V basis, and its intrinsic value is:

$$C_{DR} = \frac{<|s_{hh}+2js_{vh}-s_{vv}|^2>}{<|s_{hh}+s_{vv}|^2>} = \frac{N_c}{D_c} \quad , \qquad (A.1)$$

where the N_c and D_c are the nominator and denominator in (A.1).

Let's assume that the model is a spheroid with a mean canting angle 0° and symmetric random distribution about the vertical axis. In that case, the nominator becomes

$$N_c = \langle|s_{hh}|^2\rangle + \langle|s_{vv}|^2\rangle + 4\langle|s_{vh}|^2\rangle - 2\,Re\langle s_{vv}s_{hh}^*\rangle + 4\,Re\langle s_{vh}s_{hh}^*\rangle + 4\,Re\langle s_{vh}s_{vv}^*\rangle. \quad (A.2a)$$

The < > indicate ensemble average, which for ergodic process assumed here would equal time average (over an infinitely large time). In practice, the time average is over a finite time interval of M samples. Note that the $\mathrm{Re}\langle s_{vh}s_{hh}^*\rangle = \mathrm{Re}\langle s_{vh}s_{vv}^*\rangle = 0$ because the distribution of canting angles is assumed to be symmetric with respect to 0. Thus for this model, we have

$$N_c = \langle|s_{hh}|^2\rangle + \langle|s_{vv}|^2\rangle + 4\langle|s_{vh}|^2\rangle - 2\,Re\langle s_{vv}s_{hh}^*\rangle, \quad (A.2b)$$

and

$$D_c = \langle|s_{hh}|^2\rangle + \langle|s_{vv}|^2\rangle + 2\,Re\langle s_{vv}s_{hh}^*\rangle. \quad (A.2c)$$

The exact C_{DR} can be computed on data from fully polarimetric radar because the term $\langle|s_{vh}|^2\rangle$ in (A.2b) is available.

2) C_{DRa} proxy

The following approximation of C_{DR} has been suggested [44], [45] and is used in our paper,

$$C_{DRa} = \frac{<|s_{hh}-s_{vv}|^2>}{<|s_{hh}+s_{vv}|^2>} = \frac{N_a}{D_a}, \quad (A.3)$$

and obviously for $\langle|s_{vh}|^2\rangle$much smaller than the dominant terms ($\langle|s_{hh}|^2\rangle$ and $\langle|s_{vv}|^2\rangle$) (A.3) would equal (A.1). In the manuscript, equation (A.3) is used. Nonetheless, in practice, the intrinsic values of these terms are not available. The voltages proportional to the received electric fields are measured, and from these, the polarimetric variables are computed. Using the polarimetric variables, the proxy is computed as in [44] [45].

$$C_{DR_a} = \frac{1+Z_{dr}^{-1}-2\rho_{hv}Z_{dr}^{-1/2}}{1+Z_{dr}^{-1}+2\rho_{hv}Z_{dr}^{-1/2}}. \quad (A.4)$$

In (A.4) C_{DRa} and Z_{dr} are in linear units. The Z_{dr} may be biased by cross-coupling in the simultaneous mode of polarimetric measurements if propagation is through canted hydrometeors. That happens in oriented (other than horizontal) ice crystals and can be detected. Differential attenuation may also bias the $Z_{dr,}$ but at the 10 cm wavelength, this seldom occurs.

ACKNOWLEDGMENT

Reviews by Alexander Ryzhkov and Jeffry Snyder helped improve the paper. Robert Lee of the Radar Operation Center gave us the bias corrections of Z_{DR} and Lindsey Richardson detailed information and references about the calibration procedure. Mr. Max Olsen generously provided video images and photos of hailstones collected during this hailstorm. Funding was provided by NOAA/Office of Oceanic and Atmospheric Research under NOAA-University of Oklahoma Cooperative Agreement #NA16OAR4320072, U.S. Department of Commerce.

REFERENCES

[1] S. Lekas, "Insights on property claims for hail damage," 1 July 2014. [Online]. Available: https://www.verisk.com/insurance/visualize/insights-on-property-claims-for-hail-damage/. [Accessed 20 10 2020].

[2] Verisk, "A review of property exposure to damaging hail in 2019," 2019. [Online]. Available: https://www.verisk.com/insurance/capabilities/weather-risk/hail-and-severe-thunderstorm-risk/. [Accessed 21 10 2020].

[3] National Weather Service NOAA, "NWS 2020: Product Description Document NWS Convective Warnings with the Impact-Based Warning Format," June 2020. [Online]. Available: https://nws.weather.gov/products/PDD/PDD_Proposed_SevereThunderstormWarningCategories_2020.pdf. [Accessed 20 10 2020].

[4] Storm Prediction Center, NOAA, "CONVERTING TRADITIONAL HAIL SIZE DESCRIPTIONS," NOAA, [Online]. Available: https://www.spc.noaa.gov/misc/tables/hailsize.htm. [Accessed 21 10 2020].

[5] P. L. Heinselman and A. V. Ryzhkov , "Validation of Polarimetric Hail Detection," *Weather Forecasting,* vol. 21, pp. 839-850, 2006.

[6] J. M. Straka, D. S. Zrnic and A. V. Ryzhkov, "Bulk hydrometeor classification and quantification using polarimetric radar data: Synthesis of relations," *J. Appl. Meteorol,* vol. 39, no. 8, pp. 1341-1372, 2000.

[7] B. L. Barge and G. A. Isaac, "The shape of Albertqa hailstones," *J. Atmos. Rech,* vol. 7, pp. 11-20, 1973.

[8] V. N. Bringi, T. A. Seliga and K. Aydin, "Hail detection with differential reflectivity radar.," *Science,* vol. 225, pp. 1145-1147, 1984.

[9] K. Aydin, T. Seliga and V. Balaji, "Remote sensing of hail with a dual linear polarization radar," *J. Climate Appl. Meteorol. ,* vol. 25, no. 10, pp. 1475-1484, 1986.

[10] T. K. Depue, P. C. Kennedy and S. A. Rutledge, "Performance of the hau differential reflectivity HDR polarimetric radar hail indicator," *J. Appl. Meteor. Climatol. ,* vol. 46, pp. 1290-1301, 2007.

[11] J. C. Hubbert, V. N. Bringi, L. D. Carey and S. Bolen, "SUC - CHILL polarimetric measurements from a severe hail storm in eastern Colorado," *J Appl. Meteorol. ,* vol. 37, pp. 749-775, 1998.

[12] W. Higgs, D. Ahijevych, J. Amador, A. Barros , E. H. Berbery, E. Caetano, R. Carbone, P. Ciesielski, R. Cifelli, M. Cortez-Vaxquez and A. Douglas, "The NAME 2004 campaign and modeling strategy," *Bullet. Amer. Meteorol. Soc.,* vol. 87, no. 1, pp. 79-95, 2006.

[13] J. C. Picca and A. V. Ryzhkov, "A dual-wavelength polarimetric analysis of the 16 May 2010 Oklahoma City extreme hailstorm," *Mon. Wea. Rev,* vol. 140, pp. 1385-1403, 2012.

[14] K. L. Ortega, J. M. Kraus and A. V. Ryzhkov, "Polarimetric Radar Characteristics of Melting Hail. Part III," *J. Appl. Meteor. Climatol. ,* vol. 55, pp. 829-848, 2016.

[15] N. Balakrishnan and D. S. Zrnic, "Use of polarization to characterize precipitation and discriminate large hail," *J. Atmos Sci.,* vol. 47, pp. 1525-1540, 1990.

[16] A. V. Ryzhkov, M. R. Kumijan, S. M. Ganson and P. Zhang, "Polarimetric radar characteristics of melting hail. Part II: Practical implications," *J. Appl. Meteorol. Climatol. ,* vol. 52, pp. 2871-2886, 2013.

[17] A. V. Ryzhkov, M. R. Kumijan, S. M. Ganson and A. P. Khain, "Polarimetric radar characteristics of melting hail. Part I: Theoretical simulations using spectral microphysical modeling," *J. Appl. Meteorol. Climatol. ,* vol. 52, pp. 2849-2870, 2013.

[18] Z. Jiang , M. R. Kumijan, R. R. Schrom, I. Giammanco, T. Brown-Giammanco, H. Estes, R. Maiden and A. J. Heymsfield, "Comparisons of Electromagnetic Scattering Properties of Real Hailstones and Spheroids," *J. Appl. Meteorol. Climat. ,* vol. 58, pp. 93-112, 2019.

[19] T. A. Seliga and V. N. Bringi , "Differential reflectivity and differential phase shift: Applications in radar meteorology," *Radio Science,* vol. 13, no. 2, pp. 271-275, 1978.

[20] D. R. Longtin, C. F. Bohren and L. J. Battan, "Radar backscattering by large, spongy ice oblate spheroids," *J. Atmos. Oceanic Technol. ,* vol. 4, no. 3, pp. 355-358, 1987.

[21] H. Weickmann, "Observational data on the formation of the precipitation in cumulonimbus clouds," *Thunderstorm electricity,* pp. 66-138, 1953.

[22] K. A. Browing and J. G. Beimers, "The oblateness of large hailstones," *J. Appl. Meteorol,* vol. 6, no. 6, pp. 1075-1081, 1967.

[23] N. C. Knight, "Haulstone shape and its relation to radar interpretation of hail," *J. Climate and Appl. Meteorology,* vol. 25, no. 12, pp. 1956-1958, 1086.

[24] K. Aydin and Y. Zhao, "A computational study of polarimetric radar observabiles in hail," *IEEE Trans. Geosci. Remote Sens.,* vol. 28, pp. 412-422, 1990.

[25] I. M. Gianmmanco , T. M. Brown, M. R. Kumjian and A. J. Heymsfield, "Observations of Hailstone Sies and Shapes from IBHS Hail Measurement Program," in *27th Conference on Severe Local Storms, AMS*, Madison, WI, 2014.

[26] H. S. Park , A. V. Ryzhkov, D. S. Zrnic and K. E. Kim, "The hydrometeor classifaction for polarimetric WSR-88D; description and application to an MCS," *Wea. Forecasting,* vol. 24, pp. 730-748, 2009.

[27] M. Olson, "MASSIVE Hail in Oklahoma - April 21, 2020," Max Olson Chasing, 21 4 2020. [Online]. Available: https://www.youtube.com/watch?v=7clLyqRPCfs. [Accessed 10 3 2021].

[28] Val and Amy Castor for KWTV News 9, "VIOLENT HAIL!!! STORM NEAR ELGIN, OK 4-21-20 by Val and Amy Castor," 22 April 2020. [Online]. Available: https://www.youtube.com/watch?v=hrv1_vgIVBQ. [Accessed 15 06 2020].

[29] Storm Chasing Video, "Elk City, OK Large Damaging Hail Storm - 4/21/2020," StormChasingVIdeo.com, 21 4 2020. [Online]. Available: https://www.youtube.com/watch?v=ZFwfPbHIXXw. [Accessed 10 3 2021].

[30] R. M. Rasmussen and A. J. Heymsfield, "Melting and shedding of graupel and hail. Part I: Model physics," *J. Atmos. Sci,* vol. 44, pp. 2754-2763, 1987.

[31] WIPL d.o.o, "WIPL-D Electromagnetic Simulation Software," WIPL d.o.o, 2020. [Online]. Available: www.wipl-d.com. [Accessed 21 10 2020].

[32] B. M. Kolundzija, "Electromagnetic modeling of composite metallic and dielectric structures," *IEEE Trans. Microwave Theory and Techniques,* vol. 47, no. 7, pp. 1021-1032, 1999.

[33] D. Mirkovic, P. M. Stepanian, J. F. Kelly and P. B. Chilson, "Electromagnetic model reliably predicts radar scattering characteristics of airborne organisms," *Scientific reports,* vol. g, p. 35637, 2016.

[34] D. Mirkovic, P. M. Stepanian , C. E. Wainwright, D. R. Reynolds and M. H. Menz, "Characterizing animal anatomy and internal composition for electromagnetic modeling in radar entomology," *Remote Sens. in Ecology and Conservation,* vol. 5, no. 2, pp. 169-179, 2019.

[35] D. Mirkovic, D. S. Zrnic and A. Ryzhkov , "Full wave EM calculation of polarimetric variables for the atmospheric scatterers with nonspheroidal shape," in *2013 US National Committee of URSI National Radio Science Meeting* , Boulder, CO, 2013.

[36] E. Chobanyan, J. Notaros , V. Chandrasekar and B. Notaros , "Accurate electromagnetic modeling of melting hail," in *Proc. of 2013 US National Committee of URSI National Radio Science Meeting* , Boulder, CO, 2013.

[37] B. Notaros , V. N. Bringi, C. Kleinkort, S. B. Manic, E. Chobanyan, G. J. Huang, P. Kennedy and M. Thurai, "MoM-SIE scattering models of snow and ice hydrometeors based on 3D shape reconstructions from MASC images," in *2017 International Applied Computational Electromagnetics Society Symposioum (ACES)*, Florence, Italy, 2017.

[38] E. Chobanyan, N. J. Sekeljic, A. B. Manic, B. M. Notaros and M. M. Ilic, "Atmospheric particle scattering computation using higher order MoM-SIE method," in *2013 IEEE Antennas and Propagation Soc. International Symposioum* , Orlando, FL, 2013.

[39] E. Chobanyan, N. Sekeljic, M. M. Ilic , V. N. Bringi and B. Notaros , "Efficient and accurate computational electromagnetics approach to percipitation particle scattering analysis based on higher-order method of moments integral equation modeling," *J. Atmos. Oceanic Technol. ,* vol. 32, pp. 11745-1758, 2015.

[40] D. Mirkovic, Computational electromagnetics for polarimetric radar scatterers, Saarbrucken, Germany: LAP Lambert Academic Publishing , 2016.

[41] A. V. Ryzhkov, M. Pinsky, A. Pokorovsky and A. Khain, "Polarimetric radar observation operator for cloud model with spectral microphysics," *J. Appl. Meteorol. Cliamtol.,* vol. 50, pp. 873-894, 2011.

[42] A. R. Holt and J. Shepherd, "Electromagnetic scattering by dielectric spheroids in the forward and backward directions," *J. Phys. Math. Gen. ,* vol. 12, pp. 159-166, 1979.

[43] A. V. Ryzhkov , "Interpretation of Polarimetric Radar Covariance Matrix for Meteorological Scatterers: Theoretical Analysis," *J. of Atmos. and Ocean Techn.,* vol. 18, no. 3, pp. 315-327, 2001.

[44] V. Melnikov and S. Matrosov, "Radar Measurements of the axis ratios of cloud particles," in *36th Conf. on Radar Meteorology, AMS*, Brackenridge, CO, 2013.

[45] A. V. Ryzhkov , P. Zhang, Q. Cao, S. Matrosov, Melnikov V and M. Knight, "September measurements of circular depolarization rato woth the radar with simultaneous transmission/reception," in *Proc. 8th Eur. Conf. Radar Meteorol. Hydrol.*, Garmish-Partenkirchen, Germany, 2014.

[46] A. V. Ryhkov, S. Y. Matrosov, V. Melnikov, D. Zrnic, P. Zhang, Q. Cao and M. Knight , "Estimation of depolarization radtio using weather radars with simultaneous transmission/reception," *J. Appl. Meteorol. and Climatol. ,* vol. 56, no. 7, pp. 1797-1816, 2017.

[47] H. Akima, "A method of bivariate interpolation and smooth surface fitting based on local procedures," *Communication of ACM,* vol. 17, no. 1, pp. 18-20, 1974.

[48] M. R. Kumjian and A. V. Ryzhkov, "Polarimetric signatures in supercell thunderstorms," *J. Appl. Meteorol. Climatol. ,* vol. 47, no. 7, pp. 1940-1961, 2009.

[49] P. C. Kennedy, S. A. Rutledge, W. A. Petersen and V. N. Bringi, "Polarimtric radar observations of hail formation," *J. Appl. Meteor.,* vol. 40, pp. 1347-1366, 2001.

[50] Y. Jung, M. Xue and G. Zhang, "Simulations of polarimetric radar signatures of a supercell storm using a two-moment bulk microphysics scheme," *J. Appl. Meteor. Climatol. ,* vol. 49, pp. 146-163, 2010.

[51] V. N. Bringi, P. C. Kennedy, G. J. Huang , C. Kleinkort, M. Thurai and B. M. Notaros , "Dual-polarized radar and surface observations of a winter graupel shower with negative Zdr column," *J. Appl. Meteorol. Climatol. ,* vol. 56, no. 2, pp. 455-470, 2017.

[52] R. List, "Properties and growth of hailstones," *Thunderstorm Dynamics and Morphology,* pp. 259-276, 1985.

[53] V. N. Bringi, V. Chandrasekar, N. Balakrishnan and D. S. Zrnic, "An Examination of Propagation Effects in Rainfall on Radar Measurements at Microwave Frequences," *J. Atmos. Oceanic Technol.,* vol. 7, pp. 829-840, 1990.

[54] StormerSite.com, "Hail Report Fletcher, OK," 21 April 2020. [Online]. Available: http://www.stormersite.com/hail_reports/fletcher_oklahoma/2020. [Accessed 31 May 2020].

[55] Storm Prediction Center/NOAA, "20200421's Storm Reports (20200421 1200 UTC - 20200422 1159 UTC)," Storm Prediction Center/NOAA, 22 April 2020. [Online]. Available: https://www.spc.noaa.gov/exper/archive/event.php?date=20200421. [Accessed 10 March 2021].

[56] L. M. Richardson , J. G. Cunningham, W. D. Zittel, R. R. Lee, R. L. Ice, V. M. Melnikov , N. P. Hoban and J. G. Gebauer, "Bragg Scatter Detection by the WSR-88D. Part I: Algorithm Development," *J. Atmos. Oceanic Technol. ,* vol. 34, pp. 465-478, 2017.

[57] A. J. Illingworth, J. W. Goddard and S. M. Cherry, "Polarization studies of precipitation development in convective storms," *Quart. J. Roy. Meteor. Soc. ,* vol. 113, pp. 469-489, 1987.

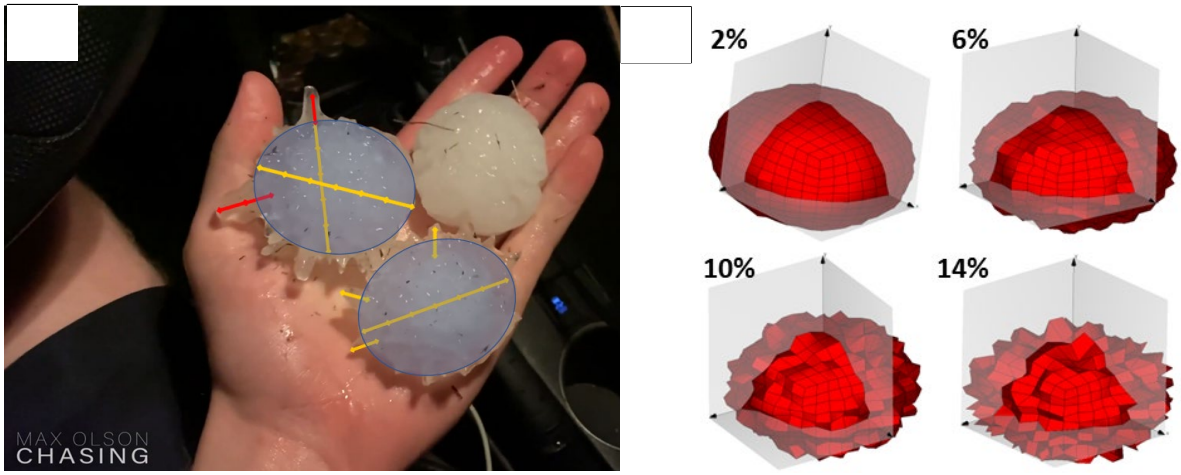

Fig. 1. a) Hailstones collected during hailstorm near Coppertone, Oklaoma on April 21st 2020 [27] (used with permission). Comparing them to the hand palm, hailstones' equatorial diameters are about 5 to 6 cm. In the photo we have a fitted spheroid and can "guage" protuberances of hailstones in fraction of diameter. b) Hailstone models with various surface roughness given as percentage of original spheroids equatorial radius.

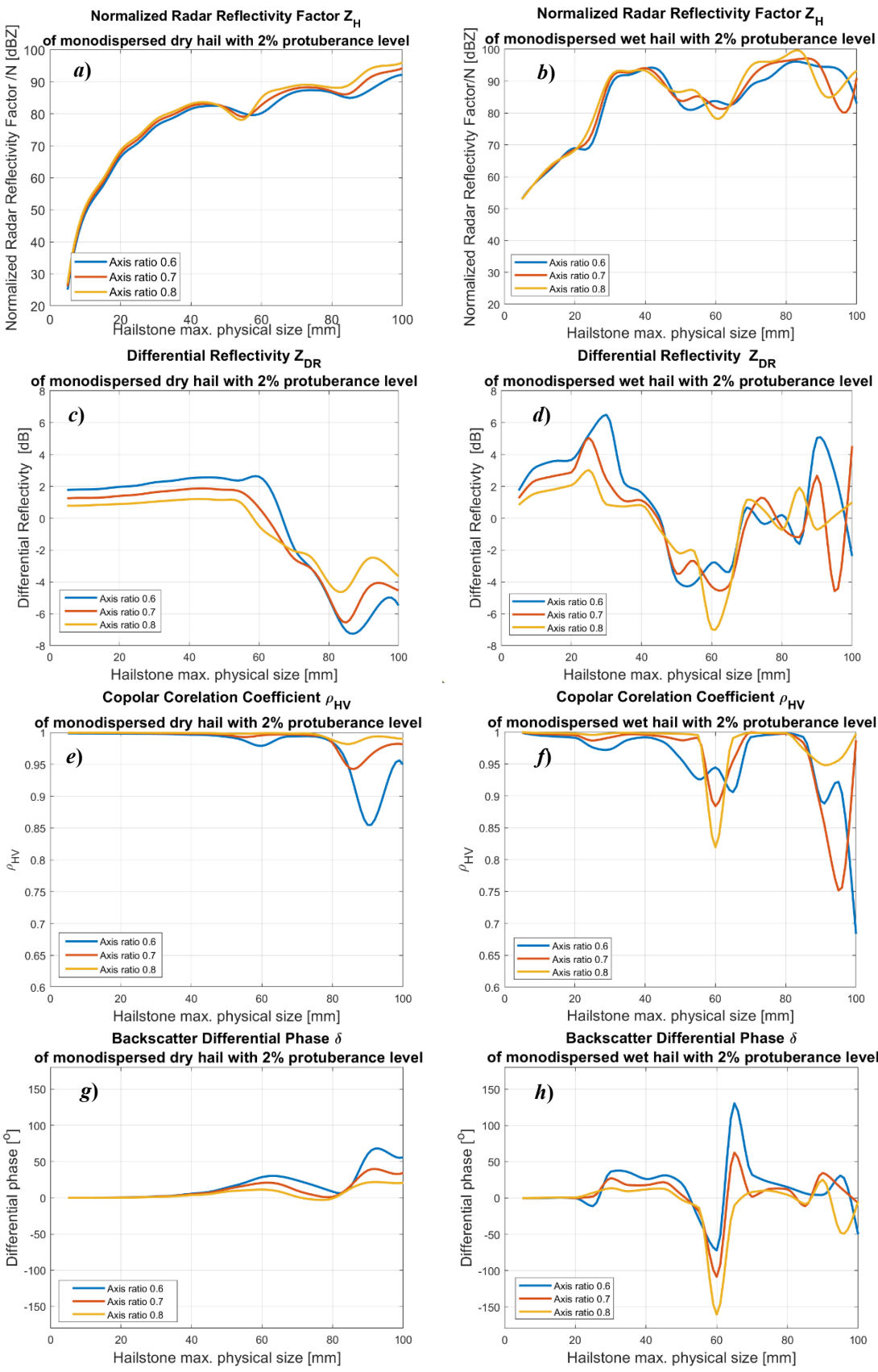
Normalized Radar Reflectivity Factor Z_H
of monodispersed dry hail with 2% protuberance level
a)
Normalized Radar Reflectivity Factor /N [dBZ]
Hailstone max. physical size [mm]
Axis ratio 0.6
Axis ratio 0.7
Axis ratio 0.8
Normalized Radar Reflectivity Factor Z_H
of monodispersed wet hail with 2% protuberance level
b)
Normalized Radar Reflectivity Factor/N [dBZ]
Hailstone max. physical size [mm]
Axis ratio 0.6
Axis ratio 0.7
Axis ratio 0.8
Differential Reflectivity Z_{DR}
of monodispersed dry hail with 2% protuberance level
c)
Differential Reflectivity [dB]
Hailstone max. physical size [mm]
Axis ratio 0.6
Axis ratio 0.7
Axis ratio 0.8
Differential Reflectivity Z_{DR}
of monodispersed wet hail with 2% protuberance level
d)
Differential Reflectivity [dB]
Hailstone max. physical size [mm]
Axis ratio 0.6
Axis ratio 0.7
Axis ratio 0.8
Copolar Corelation Coefficient ρ_{HV}
of monodispersed dry hail with 2% protuberance level
e)
ρ_{HV}
Hailstone max. physical size [mm]
Axis ratio 0.6
Axis ratio 0.7
Axis ratio 0.8
Copolar Corelation Coefficient ρ_{HV}
of monodispersed wet hail with 2% protuberance level
f)
ρ_{HV}
Hailstone max. physical size [mm]
Axis ratio 0.6
Axis ratio 0.7
Axis ratio 0.8
Backscatter Differential Phase δ
of monodispersed dry hail with 2% protuberance level
g)
Differential phase [°]
Hailstone max. physical size [mm]
Axis ratio 0.6
Axis ratio 0.7
Axis ratio 0.8
Backscatter Differential Phase δ
of monodispersed wet hail with 2% protuberance level
h)
Differential phase [°]
Hailstone max. physical size [mm]
Axis ratio 0.6
Axis ratio 0.7
Axis ratio 0.8

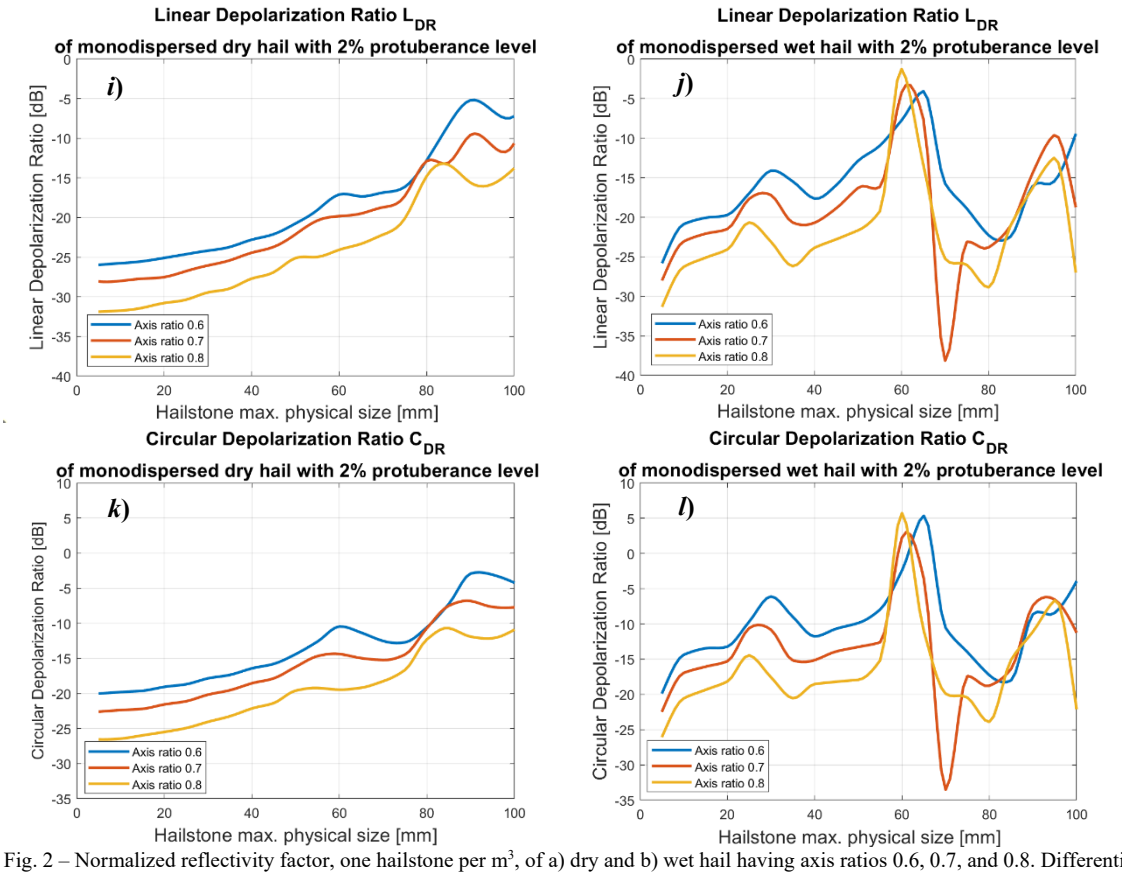

Fig. 2 – Normalized reflectivity factor, one hailstone per m^3, of a) dry and b) wet hail having axis ratios 0.6, 0.7, and 0.8. Differential reflectivity of c) dry and d) wet hail. Copolar correlation coefficient ρ_{hv} of the e) dry and f) wet hail. Backscatter differential phase of the g) dry and h) wet hail. Linear depolarization ratio L_{DR} of the i) dry and j) wet hail. Circular depolarization ratio proxy C_{DRa} of k) dry and l) wet hail.

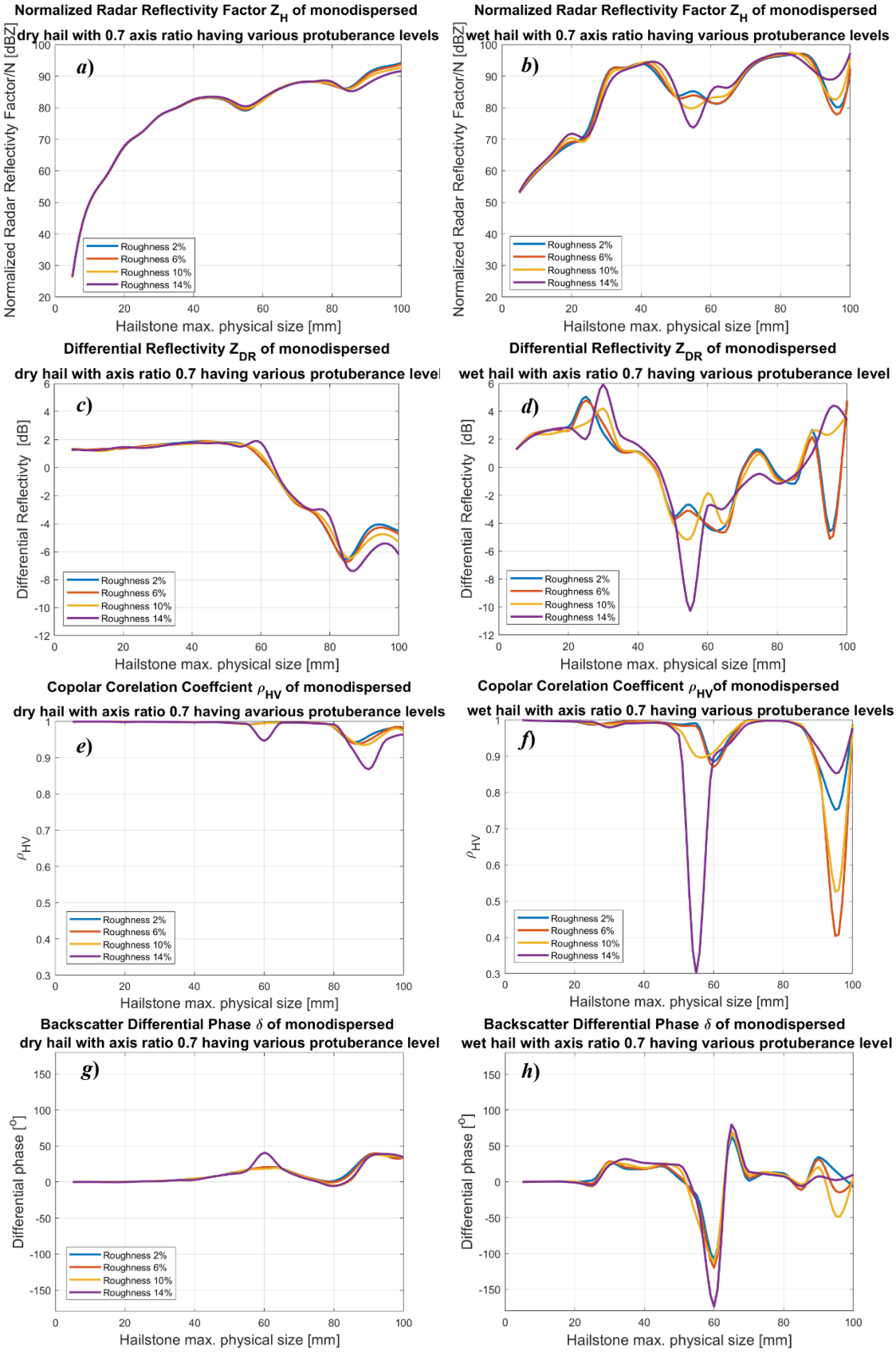
Normalized Radar Reflectivity Factor Z_H of monodispersed dry hail with 0.7 axis ratio having various protuberance levels
Normalized Radar Reflectivity Factor Z_H of monodispersed wet hail with 0.7 axis ratio having various protuberance levels
Normalized Radar Reflectivity Factor/N [dBZ]
a)
b)
Roughness 2%
Roughness 6%
Roughness 10%
Roughness 14%
Hailstone max. physical size [mm]
Differential Reflectivity Z_{DR} of monodispersed dry hail with axis ratio 0.7 having various protuberance level
Differential Reflectivity Z_{DR} of monodispersed wet hail with axis ratio 0.7 having various protuberance level
Differential Reflectivity [dB]
c)
d)
Copolar Corelation Coeffcient ρ_{HV} of monodispersed dry hail with axis ratio 0.7 having avarious protuberance levels
Copolar Corelation Coefficent ρ_{HV} of monodispersed wet hail with axis ratio 0.7 having various protuberance levels
ρ_{HV}
e)
f)
Backscatter Differential Phase δ of monodispersed dry hail with axis ratio 0.7 having various protuberance level
Backscatter Differential Phase δ of monodispersed wet hail with axis ratio 0.7 having various protuberance level
Differential phase [°]
g)
h)

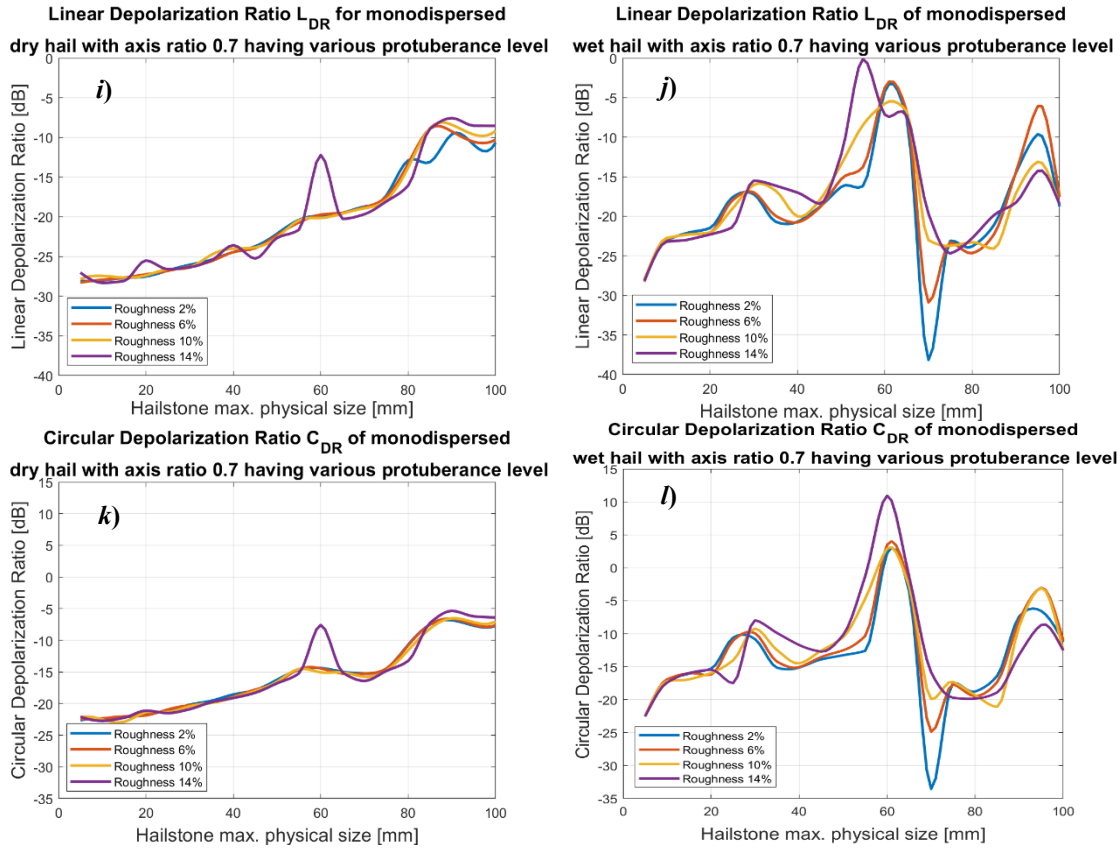

Fig. 3 – Normalized reflectivity factor, one hailstone per m^3, a) dry and b) wet hail having protuberance 2%, 6%, 10%, and 14% of its equatorial radius. Differential reflectivity of c) dry cand d) wet hail Copolar correlation coefficient ρ_{hv} of the e) dry and f) wet hail; Backscatter differential phase of g) dry and h) wet hail; Linear depolarization ratio of the i) dry and j) wet hail; Circular depolarization ratio proxy of k) dry and l) wet hail.

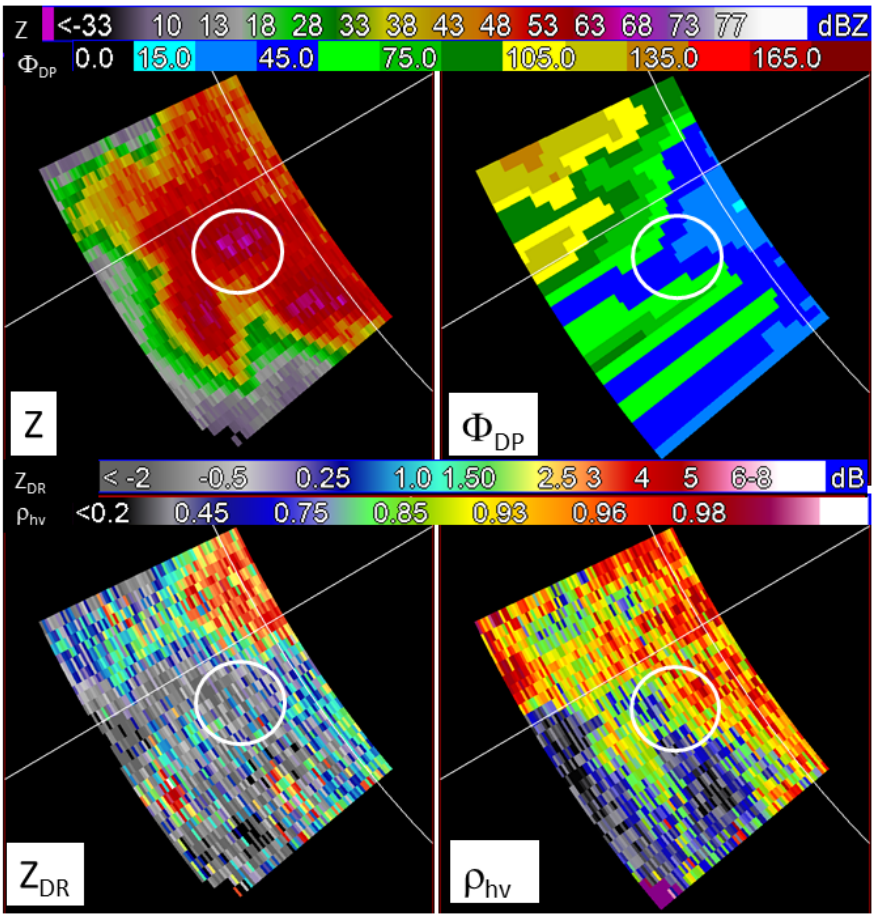

Fig. 4 – The hailstorm over Comanche county Oklahoma April 22 at 4:11 UTC observed by KTLX radar at the lowest elevation: reflectivity (Z), differential reflectivity (Z_{DR}), differential phase (Φ_{DP}), and correlation coefficient ρ_{hv}.

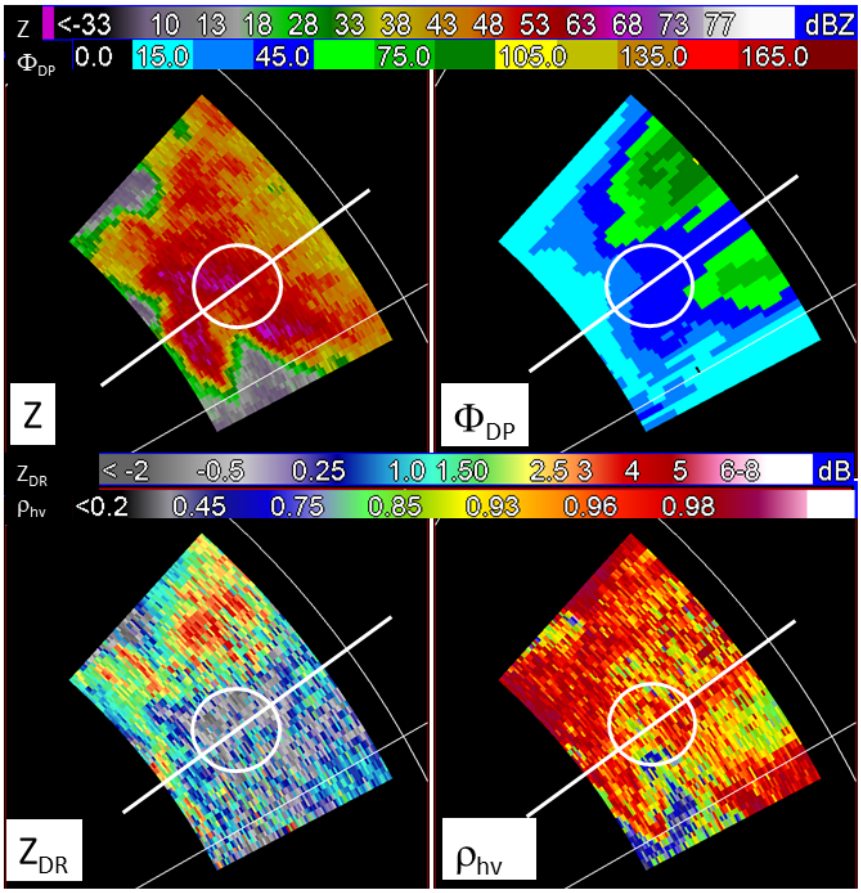

Fig. 5 – The hailstorm over Comanche county Oklahoma April 22 at 4:12 UTC observed by the KFDR radar at 0.9º elevation showing: reflectivity (Z), differential reflectivity (Z_{DR}), differential phase (Φ_{DP}), and correlation coefficient ρ_{hv}.

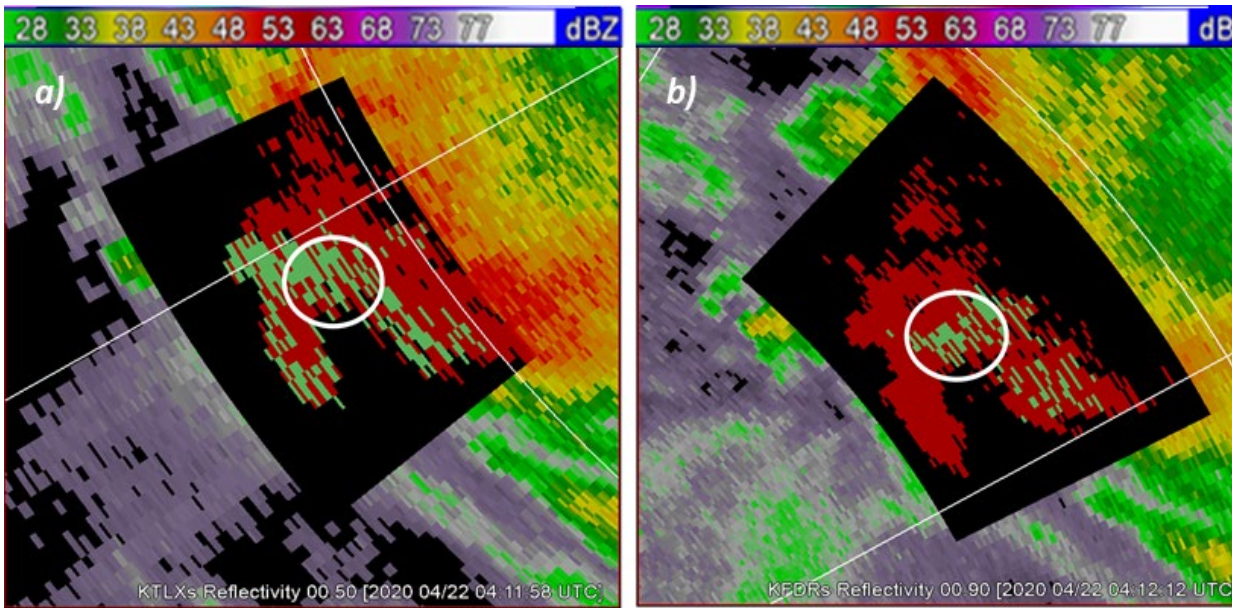

Fig. 6 - Differential reflectivity contours where Z_{DR} < -0.5 dB and Z > 53 dBZ. a) From the KTLX radar, b) from the KFDR radar.